Journal Pre-proof

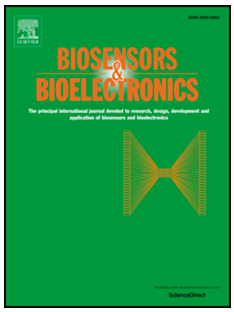

An ultrasensitive sensing platform for microRNA-155 based on H_2O_2 quenched hydroxide-dependent ECL emission of PFO Pdots

Di Liu, Xiaolong Zhang, Jinwen Zhao, Shihong Chen, Ruo Yuan

PII: S0956-5663(19)30951-0

DOI: https://doi.org/10.1016/j.bios.2019.111872

Reference: BIOS 111872

To appear in: *Biosensors and Bioelectronics*

Received Date: 25 September 2019

Revised Date: 6 November 2019

Accepted Date: 9 November 2019

Please cite this article as: Liu, D., Zhang, X., Zhao, J., Chen, S., Yuan, R., An ultrasensitive sensing platform for microRNA-155 based on H_2O_2 quenched hydroxide-dependent ECL emission of PFO Pdots, *Biosensors and Bioelectronics* (2019), doi: https://doi.org/10.1016/j.bios.2019.111872.

An ultrasensitive sensing platform for microRNA-155 based on H_2O_2 quenched hydroxide-dependent ECL emission of PFO Pdots

Di Liu, Xiaolong Zhang, Jinwen Zhao, Shihong Chen*, Ruo Yuan

Key Laboratory of Luminescence and Real-Time Analytical Chemistry (Southwest University), Ministry of Education, College of Chemistry and Chemical Engineering, Southwest University, Chongqing, 400715, P.R. China

Abstract

A strong hydroxide (OH^-)-dependent ECL emission of carboxyl functionalized-poly(9,9-di-*n*-octylfluorenyl-2,7-diyl) polymer dots (PFO Pdots) was observed at +1.25 V, which is significantly stronger than the emission at +1.95 V reported in previous work. Moreover, hydrogen peroxide (H_2O_2) can efficiently quench OH^--dependent ECL emission of PFO Pdots. Based on this discovery, a signal "off-on" ECL biosensing platform for microRNA-155 (miRNA-155) was developed. Firstly, PFO Pdots were modified onto the electrode to capture DNA duplex track-locker. In the presence of H_2O_2 in the test solution, the ECL signal of PFO Pdots was quenched to obtain a signal-off state. Subsequently, the DNA walker produced through the target miRNA-155-triggered catalytic hairpin assembly (CHA) walked along the DNA duplex track-locker to output amounts of G-rich short chain, forming a hemin/G-quadruplex. With the consumption of H_2O_2 by hemin/G-quadruplex, the ECL signal would be restored to a signal-on state, thus achieving an ultrasensitive detection of miRNA-155. The detection limit was low as 12.2 aM. Furthermore, our proposed biosensor demonstrated a tremendous selectivity and admirable stability,

*Corresponding author **Tel:** +86-23-68253172 **Fax:** +86-23-68253172
E-mail address: cshong@swu.edu.cn. (S.Chen)

and exhibited a satisfactory performance for determinating intracellular miRNA-155. The integration of excellent ECL performance of PFO Pdots without any exogenous species or dissolved O_2 as co-reactant and a highly efficient quenching effect of H_2O_2 on such an ECL emission will provide an attractive ECL platform for bioanalysis and clinical diagnosis.

Keywords: Electrochemiluminescence; Biosensor; PFO Pdots; H_2O_2; MicroRNA-155

1. Introduction

As a conjugated polymer, poly(9,9-di-*n*-octylfluorenyl-2,7-diyl) (PFO) exhibited a high carrier mobility and luminous efficiency, and an excellent thermal stability (Pecher and Mecking, 2010; Wu et al., 2008). It has drawn a wide attention, especially in the field of electrochemiluminescence (ECL) sensing, optoelectronic devices, and other biotags (Zhang et al., 2017; Zhang et al., 2018). Bard's group firstly proposed the annihilation ECL emission of PFO in benzene-MeCN solutions (Prieto et al., 2001). Since the poor water-solubility of PFO limited its application in bioanalysis, various aqueous-soluble PFO nanocomplex materials have been developed (Gao et al., 2011; Li et al., 2013; Yoo et al., 2014). In our previous works, aqueous-soluble PFO dots were prepared for detecting melamine at +1.95 V with $C_2O_4^{2-}$ as co-reactant for improving the ECL signal (Lu et al., 2015), and an ECL system based on C_{60}-PAMAM-PFO composite was constructed for detecting choline at +1.95 V with H_2O_2 as ECL co-reactant (Chen et al., 2016). However, those reported ECL emission of PFO at a high potential (+1.95 V) still suffered from an inadequate ECL intensity and insufficient stability even if introducing external co-reactants into test system. As

we know, the application of external co-reactants may result in an instability and environmental toxicity of ECL system. Fortunately, we found that the -COOH functionalized PFO polymer dots (PFO Pdots) have a stronger ECL emission at a lower potential (+1.25 V) without any exogenous species or dissolved O_2 as co-reactant, which would well address the instability and environmental toxicity problem of common ECL system with exogenous species or dissolved O_2 as co-reactant (Liu et al., 2017; Liu et al., 2007; Ma et al., 2019).

ECL quenchers, such as ferrocene (Fc), dopamine (DA), nobel metal nanoparticles, H_2O_2 and some ECL emitter as resonance energy acceptor, are widely used to achieve the signal conversion or change in ECL detection (Li et al., 2016; Liu et al., 2015; Lv et al., 2018; Richter, 2004; Shan et al., 2009). For instance, Cao and co-workers constructed a DNA biosensor based on the quenching effect of Fc on the ECL of $Ru(bpy)_3^{2+}$ through the energy transfer and electron transfer (Cao et al., 2006). Zhang and co-workers proposed a detection of microRNA-21 and microRNA-155 based on the quenching effect of DA on the ECL emission of $Ru(bpy)_3^{2+}$ and N-(4-aminobutyl)-N-ethylisoluminol (ABEI) (Zhang et al., 2018). Nevertheless, the application of these quenchers commonly involved a labelling process, which may be complex and inefficient. In the case of H_2O_2 as ECL quencher, it can be directly added into test system, or generated in situ by enzymatic reaction (Ding et al., 2019; Feng et al., 2018; Liang et al., 2017; Lv et al., 2018). For example, Lv and co-workers proposed an 8-hydroxy-2′-deoxyguanosine (8-OHdG) ECL biosensor based on the quenching effect of H_2O_2 on the ECL emission of carbon nitride nanosheets (Lv et al.,

2018). Feng and co-workers designed a DNA sensor based on the quenching of produced H_2O_2 in enzymatic reaction on the ECL of $Ru(bpy)_3^{2+}$-TPrA system (Feng et al., 2018). In addition, H_2O_2 has also been reported as a quencher for $Ir(ppy)_3^{2+}$-TPrA, black phosphorus (BP)-TPrA and other ECL systems (Ding et al., 2019; Liang et al., 2017). However, in these strategies with H_2O_2 as quencher, the ECL emission usually involved the application of exogenous species or dissolved O_2 as co-reactant. Therefore, it is of great significance to expand the quenching effect of H_2O_2 on the ECL systems excluding exogenous species or dissolved O_2 as co-reactant.

MicroRNAs (miRNAs), a class of non-coding single-stranded RNA molecules encoded by endogenous genes, which was involved in several aspects of the innate immune responses, and could be applied to the detection, diagnosis, prognosis and possible treatment of human cancers (Bartel, 2004; Johnson et al., 2005; Tricoli and Jacobson, 2007; Yu et al., 2018). However, the detection of miRNAs was a challenge because of the ultra-low abundance, short sequence and high sequence similarity of miRNAs (Gu et al., 2017; Li et al., 2019; Qi et al., 2018). Hence, it is significant to develop rapid, accurate, and sensitive miRNA detection strategies for cancer prevention (Bi et al., 2017; Chen et al., 2018; Kilic et al., 2018; Yue et al., 2019). Due to low background, high sensitivity and wide dynamic range, the ECL strategy has attracted more and more attention in the detection of nucleic acids (Huo et al., 2018; Liao et al., 2018; Lu et al., 2018). For instance, Liu and co-workers applied a bi-pedal DNA walker signal amplification strategy to construct an ECL biosensor for detecting

miRNA-21 (Liu et al., 2018). Zhang and co-workers also constructed an ECL strategy based on three-dimensional (3D) DNA nanomachine for miRNA detection (Zhang et al., 2018). Undoubtedly, the introduction of nucleic acid amplification strategies based on DNA nanomachines would endow the ECL sensing with a better performance and expand the application field of ECL detection. However, these strategies generally involved exogenous co-reactants or dissolved O_2, which may result in the toxic, instability and inefficiency problem (Gao et al., 2011; Liu et al., 2017; Liu et al., 2007). Therefore, it is very valuable to develop a miRNA sensing platform excluding exogenous co-reactants or dissolved O_2.

Based on the in-depth exploration of the ECL properties of PFO Pdots at +1.25 V, an "off-on" sensing strategy was exploited for miRNA detection. Firstly, PFO Pdots were modified onto the electrode surface for loading the oligonucleotide. H_2O_2 was added into the detection system to quench the strong initial signal of PFO Pdots, giving a signal-off state. Then, the DNA Walker, which was liberated from the catalytic hairpin assembly (CHA) reaction triggered by target miRNA-155, walked on the electrode surface over and over in the presence of Pb^{2+}. After N cycles, a mount of short G-rich strands was obtained. Short G-rich strands captured hemin to form a hemin/G-quadruplex, which consumed quencher H_2O_2 to obtain a signal-on state, thus achieving the ultrasensitive detection of miRNA-155. The detection of miRNA-155 in cell lysates was investigated. Our proposed ECL strategy not only well overcame the defect of exogenous species or dissolved O_2 as co-reactant, but also explored the ECL quenching effect of H_2O_2 on the hydroxide-dependent ECL emission, thus expanding

the application of PFO Pdots in ECL field and providing a promising and attractive bioanalysis platform for miRNAs.

2. Experimental

2.1. Apparatus, reagents and materials

Detailed information on the apparatus, reagents and materials used in this work is presented in the **Supplementary Material**. The sequences and modifications of RNA and DNA oligonucleotides are listed in Table S1 in the **Supplementary Material**.

2.2. Preparation of PFO Pdots

PFO Pdots were prepared according to the literatures with minor modifications (Chen et al., 2017; Sun et al., 2012). Typically, 5.0 mL of solution A (5.0 mg of PFO in tetrahydrofuran (THF)) and 1.0 mL of solution B (1.0 mg of poly(styrene-*co*-maleicanhydride) (PSMA) in THF) were prepared as stock solutions, respectively. Then, the solution A and solution B were mixed together in the ultrasound system (5:1, *v*/*v*). After 2 h, the mixed solution was quickly added to 10 mL of deionized water with ultrasound. Finally, solvent THF was removed with argon stripping. After filtration through a 400 nm filter, the PFO Pdots dispersion was obtained. Scanning electron microscope (SEM), UV-visible spectrum, fluorescence spectrum and Fourier transform infrared (FT-IR) spectroscopy were used to characterize the synthesis of PFO Pdots, and the results are described in the **Supplementary Material** and corresponding figures are depicted as Fig. S1.

2.3 Assembly of the biosensor

The construction process of the miRNA-155 biosensor is presented in Scheme 1.

After processed according to the literatures (Liao et al., 2018; Lu et al., 2018), the bare glassy carbon electrode (GCE, 4 mm in diameter) was modified with 10 μL of PFO Pdots dispersion (0.10 mg/mL). Subsequently, 5 μL of EDC solution was incubated on the PFO Pdots/GCE about 15 min to activate the carboxyl group on the surface of PFO Pdots. And then 10 μL of DNA duplex track-locker (T-L, 2.0 μM) and 5 μL of NHS were cast onto the modified electrode, aiming at cross-linking the DNA duplex track-locker onto the surface of PFO Pdots/GCE. After rinsed with PBS to remove excess EDC/NHS and nonspecifically adsorbed DNA, the electrode was further incubated with bovine serum albumin (BSA) (0.25 %) for 30 min to block the remaining active sites of the electrode and then rinsed by PBS to obtain BSA/T-L/PFO Pdots/GCE. Later, the target with different concentrations was mixed with the prepared hairpin H1 and H2 in Tris-HCl buffer (pH 7.4, containing 8.0 μM Pb^{2+}). The resultant mixture (15 μL) was dropped onto the surface of the BSA/T-L/PFO Pdots/GCE and incubated under 37 □ for 160 min. After washing off the excess DNA strand on the electrode surface with PBS, the electrode was incubated with 5 μL of hemin aqueous solution (0.5 μM, containing K^{+}) for 40 min to form hemin/G-quadruplex. The preparation of DNA duplex, Hairpin H1 and H2 used during the assembly of biosensor is presented in the **Supplementary Material**. The native PAGE was also employed to characterize the related reaction of DNA walker and the corresponding results are described in **Supplementary Material** and corresponding figures are depicted as Fig. S2. The assembly of the biosensor was characterized by cyclic voltammetry (CV), electrochemical impedance spectroscopy

(EIS) and ECL. The corresponding results are described in the **Supplementary Material** and corresponding figures are shown as Fig. S3.

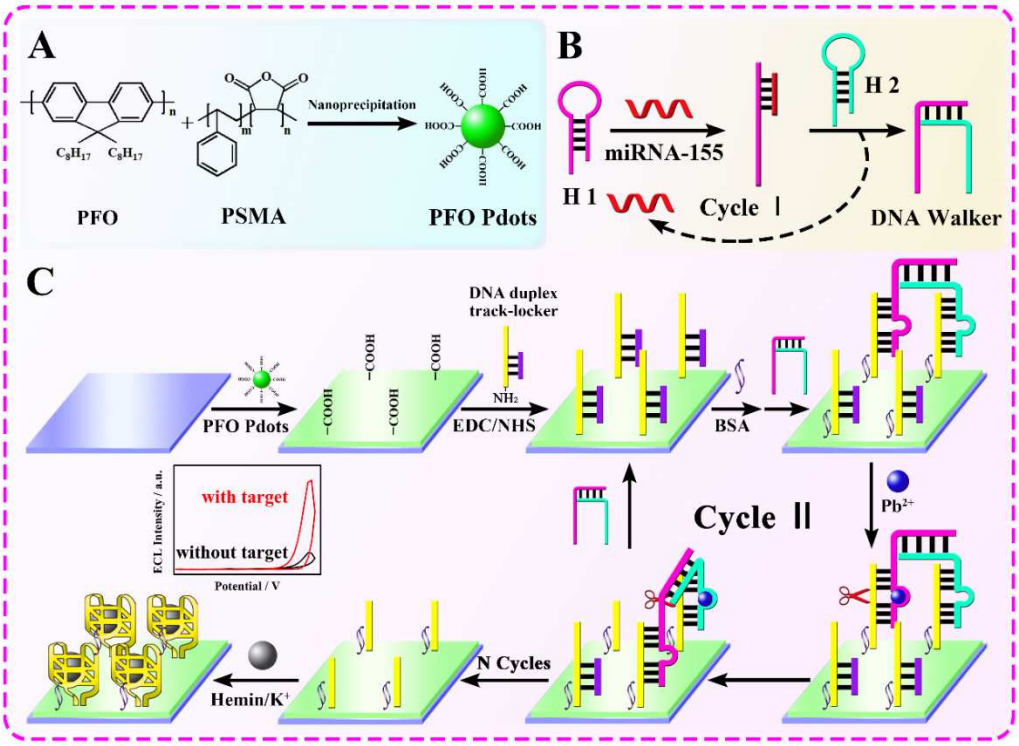

Scheme 1. (A) Schematic illustration of materials preparation, (B) the concept of the DNA walker, and (C) the fabrication of miRNA-155 biosensor.

3. Results and discussion

3.1. Effect of the scanning potential on the ECL emission of PFO Pdots

Generally, PFO based ECL system was performed the ECL detection with a scanning potential range of 0 – 2.0 V, and in this case, the emission potential was clearly detected at +1.95 V (Chen et al., 2016; Lu et al., 2015). Now, we found that the scanning potential would significantly affect the ECL emission of PFO Pdots, which was confirmed by the following four aspects.

Firstly, under the scanning potential range of 0 – 2.0 V, the ECL Intensity-Potential curves of PFO Pdots modified GCE (PFO Pdots/GCE) were

carefully recorded with the change of scanning cycles and the results are demonstrated in Fig. 1A. When the first scanning cycle was performed in PBS (pH 7.4), two ECL emissions were clearly detected, which were ECL-1 with a peak value at +1.25 V and ECL-2 with a peak value at +1.95 V (Fig. 1A, red curve). Moreover, ECL-1 at +1.25 V was much stronger than ECL-2 at +1.95 V. When the second scanning cycle was performed, ECL-1 completely disappeared, namely the emission at +1.25 V disappeared, and only ECL-2 (+1.95 V) was observed (Fig. 1A, black curve). In fact, the results with more scanning cycles were similar to that with the second scanning cycle (data not shown), namely, only one ECL emission (+1.95 V) can be detected when the scanning cycles exceeded 2. Secondly, when ECL detection was performed at PFO Pdots/GCE with a scanning potential range of 0 – 1.25 V in PBS (pH 7.4), a strong ECL emission could be always detected at +1.25 V no matter how the scanning cycle changed (data not shown), indicating that the ECL emission at +1.25 V is almost unaffected by scanning cycles in the case of the scanning potential range of 0 – 1.25 V. Thirdly, once the PFO Pdots/GCE was performed a scanning cycle during 0 – 2.0 V, the ECL emission at +1.25 V cannot be detected even if the potential was reset to 0 – 1.25 V. Fourthly, in order to thoroughly investigate the effect of scanning potential on the ECL emissions, the low potential was always set to 0 V, and the high potential was changed from +0.8 V to +2.0 V to record the ECL Intensity-Potential curves at PFO Pdots/GCE in PBS (pH 7.4). Here, considering the possible difference in ECL curves between the first scanning cycle and the second scanning cycle, under the different scanning potential range, the ECL curves with the

second scanning cycle were always selected for discussion and the results are exhibited in Fig. 1B. As seen, with the change of scanning potential range, an obvious difference in ECL response signal was noticed. When the scanning potential range was set as 0 – 0.8 V, 0 – 0.9 V or 0 – 1.0 V, no distinct ECL emission was detected. And a strong ECL emissions can be detected when the high potentials ranged between +1.1 V and +1.5 V. When the high potential exceeded +1.6 V, a significantly weakened ECL signal was detected. It's worth noting that the ECL intensity with the scanning potential of 0– 2.0 V was higher than those with 0 – 1.6 V, 0 – 1.7 V, 0 – 1.8 V, and 0 – 1.9 V, which was consistent with our previous works (Chen et al., 2016; Zhang et al., 2017). Moreover, ECL signal with the scanning potential of 0 – 1.2 V or 0 – 1.3 V was much stronger than that with a scanning potential range of 0 – 2.0 V.

A possible explanation for the above experimental phenomena is that the ECL emission of PFO Pdots with a scanning potential of 0 – 1.25 V is different from the ECL emission with the scanning potential of 0 – 2.0 V. To confirm this speculation, the cyclic voltammetry (CV) response was detected at PFO Pdots/GCE in MeCN containing 0.10 M $TBAPF_6$ as an electrolyte. Fig. S4 demonstrates the cyclic voltammograms (CVs). An obvious oxidation wave was clearly detected at +1.52 V when the first CV scanning was performed. However, the oxidation wave at +1.52 V completely disappeared when the second CV scanning was performed, which was consistent with previous ECL results (Fig. 1A). Therefore, it was speculated that the strong ECL emission of PFO Pdots at +1.25 V was assigned to the excited-state composite of the PFO Pdots, while the emission at +1.95 V was arisen from

intra-polymer emission of PFO Pdots. The ECL emission of the excited-state composite of PFO Pdots was much stronger than that of intra-polymer emission, which was consistent with the reported excimer emission of polymer materials (Prieto et al., 2001). The ECL emission of PFO Pdots at +1.25 V required less energy, and high potential scanning may destroy the excited-state composite. Once a scanning with the potential exceeding +1.52 V was performed, an irreversible damage has occurred at the excited complex. Thus, once the first scanning cycle was performed in the potential range of 0 – 2.0 V, the emission of PFO Pdots at +1.25 V (ECL-1) would completely disappear. Namely, the scan potential could not exceed +1.5 V if the emission at +1.25 V is to be always detected.

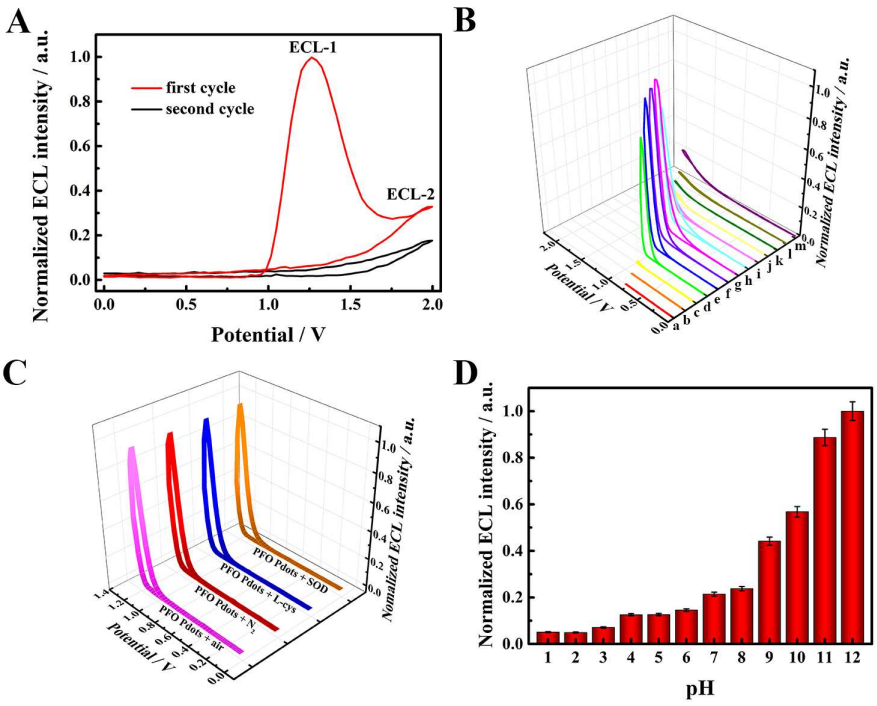

Fig. 1. (A) ECL behaviors of PFO Pdots/GCE with scanning potential from 0 to +2.0 V; (B) ECL signals of PFO Pdots/GCE with different scanning potential range: (a) 0 – 0.8 V, (b) 0 – 0.9 V, (c) 0 – 1.0 V, (d) 0 – 1.1 V, (e) 0 – 1.2 V, (f) 0 – 1.3 V, (g) 0 – 1.4 V, (h) 0 – 1.5 V, (i) 0 – 1.6 V, (j) 0 – 1.7 V, (k) 0 – 1.8 V, (l) 0 – 1.9 V, and (m) 0 – 2.0 V; (C) ECL behaviors of PFO Pdots/GCE under different conditions; (D) ECL response of PFO Pdots/GCE in PBS with

different pH (scanning potential: 0 – 1.25 V; scanning rate: 0.30 V/s; the voltage of photomultiplier tube: 800 V).

3.2. Exploration of the ECL mechanism of PFO Pdots

For the strong ECL emission of PFO Pdots at +1.25 V in PBS (pH 7.4) without any exogenous co-reactant, ECL mechanism was studied under the scanning potential range of 0 – 1.25 V. Firstly, we explored the effect of dissolved O_2 since it usually served as a co-reactant to enhance ECL signals (Liu et al., 2017). As seen from Fig. 1C, no obvious difference in the ECL signals of PFO Pdots was observed between air saturation (dissolved O_2 atmosphere) and N_2 atmosphere, indicating that the dissolved O_2 didn't serve as a co-reactant in this ECL system. Secondly, the effect of active oxygen species ($O_2^{\bullet-}$ and $OH^{\bullet}$) produced during potential scanning was investigated. Superoxide dismutase (SOD) and L-cysteine (L-cys) were used to remove active oxygen species in test solution (Deng et al., 2011; Nistri et al., 2015). As exhibited in Fig. 1C, compared with the ECL signal in the case of dissolved O_2 atmosphere or N_2 atmosphere, the ECL emission of PFO Pdots didn't exhibit an obvious change with SOD as the purifier of $O_2^{\bullet-}$ or with L-cys as the scavenger of $O_2^{\bullet-}$ and $OH^{\bullet}$, thus the action of active oxygen species in the ECL reaction of PFO Pdots was excluded.

Next, the ECL signals of PFO Pdots/GCE were examined in PBS at different pH to further explore the effect of hydroxide (OH^-) on the ECL emission of PFO Pdots. As exhibited in Fig. 1D, the ECL responses of PFO Pdots/GCE increased significantly with increasing pH from 1 to 12. This may be ascribed to the fact that traces of OH^- in PBS were involved in ECL route, and acted as an intermediate to react with PFO Pdots. The possible ECL mechanism of PFO Pdots was depicted in Fig. 2E. Firstly,

PFO Pdots were oxidized on the surface of GCE to give a polymer radical cation [PFO Pdots]$^{+\bullet}$. Then, in the presence of OH^-, the protons of [PFO Pdots]$^{+\bullet}$ radical were eliminated to produce a reductive intermediate radical [PFO Pdots]$^{\bullet}$, which reacted with [PFO Pdots]$^{+\bullet}$ to generate an excited-state species [PFO Pdots]*. [PFO Pdots]* further reacted with PFO Pdots to yield excited-state composite species [PFO Pdots-PFO Pdots]*, and finally creating ECL emissions. Similar enhancing effect of OH^- on the ECL emission has been observed at poly[(9,9-dioctylfluorenyl-2,7-diyl)-*co*-(1,4-benzo-{2,1'-3}-thiadiazole)] (PFBT) and poly[9,9-bis(3'-(N,N-dimethylamino)propyl)-2,7-fluorene]-alt-2,7-(9,9-dioctylfluoren e)] (PFN) (Luo et al., 2019; Ma et al., 2019). As is well known, the concentration of OH^- in a buffer system (PBS) is easily controlled to a relatively constant value, which endows the OH^--dependent ECL emission of PFO Pdots (at +1.25 V) a high stability and repeatability.

3.3. The effect of H_2O_2 on the ECL emission

The effect of H_2O_2 on the ECL emission of PFO Pdots was also explored under the different scanning potentials. The low potential was always set to 0 V, and the high potential was changed from +0.8 V to +2.0 V to record the ECL response of PFO Pdots/GCE in PBS (pH 7.4) without and with H_2O_2. The blue columns and pink columns in Fig. 2A corresponded to the ECL signals detected in PBS without and with 10 mM H_2O_2, respectively. It can be clearly seen that H_2O_2 has a different effect on the ECL response of PFO Pdots/GCE under the different scanning potentials. When the high potential was lower than +1.0 V or higher than +1.6 V, H_2O_2 served as

a co-reactant to enhance the ECL signal. In fact, the enhancing effect of H_2O_2 on the ECL signal at +1.95 V has been reported in our previous work (Chen et al., 2016; Chen et al., 2017). However, when the high potential changed between +1.1 V and +1.5 V, the function of H_2O_2 wasn't to enhance the ECL signal, but to quench the ECL signal. Impressively, quenching efficiency of H_2O_2 was significantly higher than its enhancement efficiency on the ECL emission of PFO Pdots.

To investigate the quenching mechanism of H_2O_2, the ECL and corresponding CV response curves of PFO Pdots/GCE were detected in PBS (pH 7.4) without (Fig. 2B) and with (Fig. 2C) 10 mM H_2O_2 under the scanning potential of 0 – 1.25 V. As recorded in Fig. 2C, while the H_2O_2 quenched the ECL response at +1.25 V (ECL curves), the CV current increased significantly (CV curves). In addition, to further explore the effect of H_2O_2 on the ECL of PFO Pdots, the holes (h^+) of PFO Pdots were detected using the Electron Paramagnetic Resonance (EPR) and Fig. 2D exhibits corresponding EPR spectra. As seen, in the dark, both the system PFO Pdots (curve 2) and the system PFO Pdots + H_2O_2 (curve 4) presented a strong TEMPO radical triplet signal, indicating that hardly any photogenerated h^+ was produced at PFO Pdots and H_2O_2 also had no effect in the absence of irradiation. Under the irradiation, the signal from TEMPO radical triplet of PFO Pdots almost disappeared (curve 1), indicating a produce of photogenerated h^+ at PFO Pdots. When H_2O_2 was added in PFO Pdots system, the EPR spectra demonstrated a significant increase in TEMPO radical triplet signal (curve 3). The reason may be as follows. Under the irradiation, H_2O_2 was oxidized by the photogenerated h^+ (Du et al., 2019), and leading to a decrease in the

297 amount of h^+. Thus the ECL emission of PFO Pdots was blocked. According the
298 results of CV and EPR and previous reports (Liang et al., 2017; Lv et al., 2018), it
299 was speculated that the quenching effect of H_2O_2 on the ECL of PFO Pdots may be
300 owing to the synergistic effect of the electron transfer and the reaction between the
301 excited state species and H_2O_2. The possible quenching mechanism of H_2O_2 on the
302 ECL was depicted in Fig. 2E.

303 Since the ECL emission of PFO Pdots at +1.25 V was not only OH^--dependent
304 ECL, but also could be efficiently quenched by H_2O_2. Our proposed method is making
305 use of this ECL feature to construct a biosensor for detecting miRNA-155.

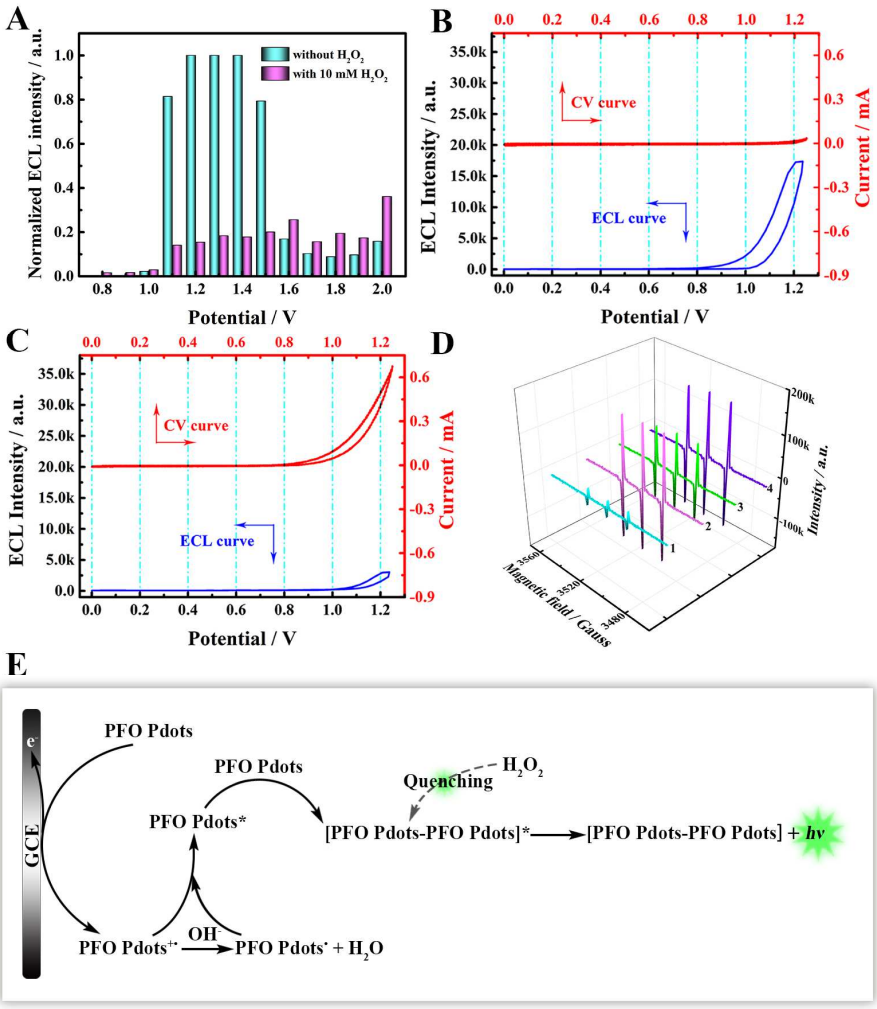

306

Fig. 2. (A) Effect of H_2O_2 on ECL response of PFO Pdots/GCE; ECL and CV curves of PFO Pdots/GCE without (B) and with (C) 10 mM H_2O_2 (scanning potential: 0 – 1.25 V; scanning rate: 0.30 V/s; the voltage of photomultiplier tube: 800 V); (D) EPR spectra of radical adducts trapped by TEMPO (h^+) in PFO Pdots (1, light; 2, dark) and PFO Pdots + H_2O_2 (3, light; 4, dark); (E) Possible ECL mechanism of PFO Pdots and quenching mechanism of H_2O_2

3.4. ECL Spectra of PFO Pdots

Fig. 3A and Fig. 3B present the spooled ECL spectra and the heat map image of PFO Pdots/GCE in PBS containing 20 mM triethylamine (TEA) under the scanning potential of 0 – 1.25 V, respectively. The maximum ECL emission was detected at 520 nm and it showed a red shift when compared to the fluorescence emission spectra (439.6 nm, 467.8 nm, and 499.2 nm), which may be ascribed to the fact that the formation of excited-state excimer species resulted in a decreasing energy (Prieto et al., 2001).

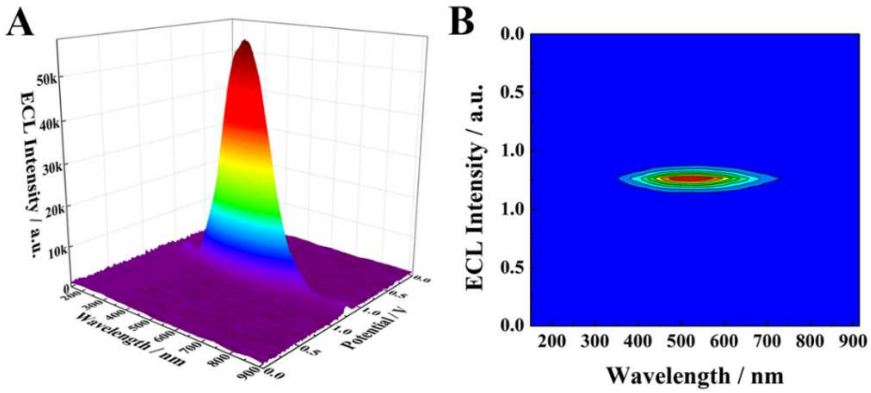

Fig. 3. Spooled ECL spectra (A) and the heat map image (B) of PFO Pdots/GCE in PBS containing 20 mM TEA under the scanning potential from 0 to 1.25 V.

3.5. The detection of miRNA-155

The concentration of quencher H_2O_2 was optimized to obtain a low background signal. And the concentrations of hemin and Pb^{2+}, as well as the incubation time of DNA Walker were optimized to achieve optimal performance of miRNA-155

biosensor. The corresponding results are described in the **Supplementary Material** and corresponding figures are depicted as Fig. S5. The optimal experimental conditions were as follows: (a) optimal concentration of H_2O_2 was 14.0 mM; (b) optimal concentration of hemin was 0.5 μM; (c) optimal concentration of Pb^{2+} was 8.0 μM; (d) optimal incubation time of DNA Walker was 160 min.

The ECL response of the proposed biosensor to miRNA-155 was explored in 3.0 mL of 0.10 M PBS (pH 7.4) containing 14.0 mM H_2O_2 under optimized conditions. As shown in Fig. 4A, as the target concentration increased from 50 aM to 1.0 nM, the ECL intensity was gradually increased as we expected. The reason for the increase in ECL signal was that hemin/G-quadruplex formed on the surface of GCE consumed H_2O_2 and generated OH^- in accordance with the following equations (Deng et al., 2013; Lv et al., 2018; Zhou et al., 2013):

hemin/G-quadruplex (Fe^{III}) + e^- → hemin/G-quadruplex (Fe^{II}) (1)

hemin/G-quadruplex (Fe^{II}) + 1/2 H_2O_2 →hemin/G-quadruplex (Fe^{III}) + OH^- (2)

The ECL signals showed an excellent linear relationship with the logarithm of the miRNA-155 concentration. The corresponding calibration curve is shown in Fig. 4B, and the regression equation was expressed as I (a.u.) = 6307.25 + 946.10 log (c/pM), and the correlation coefficient value (R) was 0.9980 (I as the ECL intensity and c as the concentration of miRNA-155). In addition, the detection limit of miRNA-155 was 12.2 aM, which was calculated according to the formula LOD = $3S_B/m$ (m is the slope of the corresponding calibration curve; S_B is the standard deviation of the blank). Moreover, compared with the previous works, our prepared

biosensor in this work exhibited an excessive potential for ultrasensitive detection of miRNA-155 (Table 1).

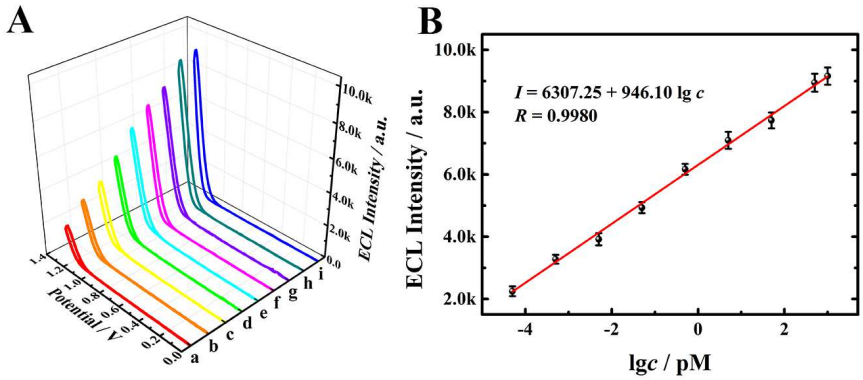

Fig. 4. (A) ECL intensity-potential curves for various concentration of miRNA-155: (a) 50 aM, (b) 500 aM, (c) 5 fM, (d) 50 fM, (e) 500 fM, (f) 5 pM, (g) 50 pM, (h) 500 pM, and (i) 1 nM in 0.10 M PBS (pH 7.4, containing 14.0 mM H_2O_2). (B) calibration curve between ECL intensity and logarithm of target miRNA-155 concentration (scanning potential: 0 – 1.25 V; scanning rate: 0.30 V/s; the voltage of photomultiplier tube: 800 V).

Table 1 The comparison of different methods for miRNA-155 detection.

Methods	Detection limit	Dynamic range	Ref.
Fluorescence	1.0 fM	1.0 fM – 100 nM	(Zhang et al., 2017)
Electrochemistry	10 fM	5.0 fM – 5.0 pM	(Koo et al., 2016)
ECL	0.3 fM	1.0 fM – 100 pM	(Zhang et al., 2015)
ECL	3.3 aM	10 aM – 5.0 pM	(Luo et al., 2019)
ECL	12.2 aM	50 aM – 1.0 nM	This work

3.6. The stability, selectivity, reproducibility, and practical application of biosensor

The stability of the biosensor was investigated by detecting the ECL signal of the biosensor with miRNA-155 (50 fM) under continuous cyclic scan in 3.0 mL PBS (pH 7.4). As seen in Fig. 5A, no obvious change was observed after nine cycles of scanning and the RSD of 1.39 % was obtained, indicating that the biosensor has an excellent stability.

To explore the selectivity of the prepared biosensor, miRNA-141, miRNA-126,

and miRNA-21 were selected as possible interferents. The ECL signals were measured under the blank, miRNA-141, miRNA-126, miRNA-21, and mixture (miRNA-155, miRNA-141, miRNA-126, and miRNA-21) system, respectively. As shown in Fig. 5B, even if the concentration of the interferents was 100-times higher than that of target miRNA, no significant interference was observed at the interferents. Only in the presence of the target, a strong ECL response could be observed, indicating a satisfactory selectivity.

The inter-assays and intar-assays of the miRNA-155 biosensors were further investigated using four biosensors prepared in various batches and in the same batch, respectively. As seen from Fig. 5C, the RSD of inter-assays and intar-assays was all below 5 %, indicating that the biosensor has a significant reproducibility.

The expression of miRNA-155 in different biological cell lysates was examined to further validate the practicality of the biosensor, including cervical cancer cells (Hela) and human breast cancer cells (MCF-7) lysates. Firstly, the cell samples were processed by a commercial miRNA extraction kit after cell counting (a detailed preparation process is described in the **Supplementary Material**). As shown in Fig. 5D, the ECL response gradually increased as the cell numbers increased, exhibiting a significant expression level of target miRNA-155 from MCF-7. However, in HeLa cells, the obviously lower ECL responses were observed (b-f), demonstrating a relatively low expression level compared to MCF-7. The above results were consistent with the previous research (Luo et al., 2019; Yue et al., 2019; Zhang et al., 2018), further indicating that the proposed quantification of miRNA-155 in cancer

391 cells possesses a potential for clinical diagnosis of cancers.

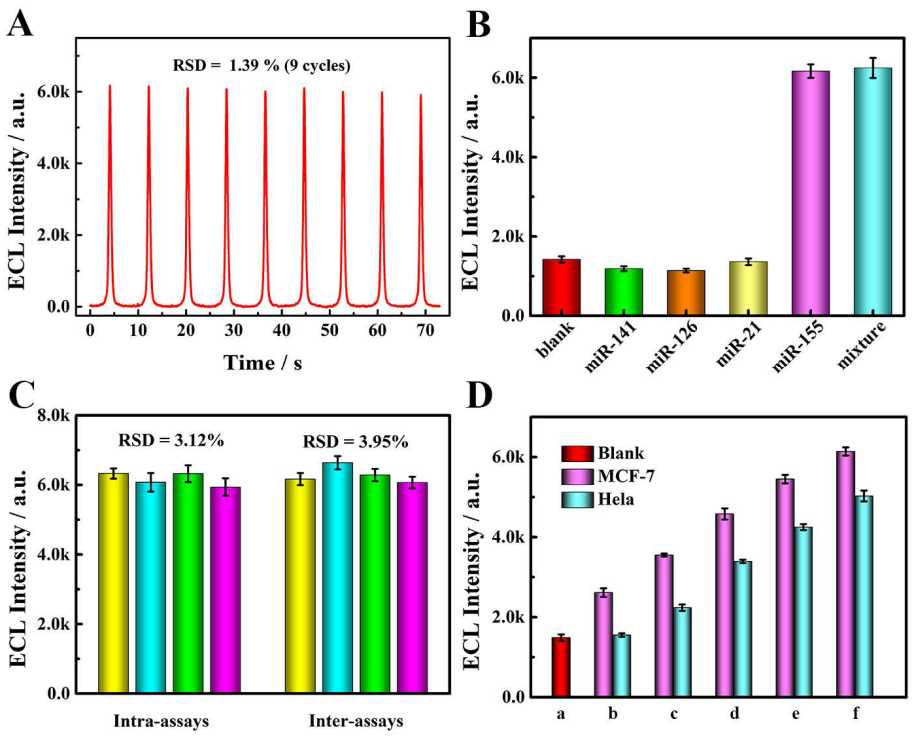

392

393 **Fig. 5.** (A) ECL intensity-time curve of the biosensor under scanning 9 cycles in PBS (0.10 M, pH
394 7.4) containing 14.0 mM H_2O_2 with miRNA-155 concentration of 0.5 pM; (B) The selectivity and
395 (C) reproducibility of the biosensor; (D) ECL response of the prepared biosensor for miRNA-155
396 extracted from MCF-7 and HeLa cells with different numbers (blank, 10, 10^2, 10^3, 10^4, and 10^5
397 cells), (scanning potential: 0 – 1.25 V; scanning rate: 0.30 V/s; the voltage of photomultiplier tube:
398 800 V).

399

400 **4. Conclusion**

401 PFO polymer dots (PFO Pdots) were found to exhibit a strong ECL emission at a
402 lower potential (+1.25 V) without any exogenous co-reactants. Based on the thorough
403 investigation on the ECL mechanism, an OH^--dependent ECL emission characteristic
404 was confirmed. Furthermore, such an ECL emission could be efficiently quenched by
405 H_2O_2. The controllability of OH^- concentration in PBS and the non-toxicity of OH^-
406 endowed OH^--dependent ECL emission a superior performance over other ECL
407 emissions with exogenous species or dissolved oxygen (O_2) as co-reactant. The

constructed biosensor with PFO Pdots as luminophore and H_2O_2 as ECL quencher achieved the sensitive detection of miRNA-155 with a detection limit as low as 12.2 aM. The integration of PFO Pdots and H_2O_2 significantly extends the application of PFO, and provides an attractive ECL platform for bioanalysis.

Acknowledgements

This work was supported by National Natural Science Foundation of China (21775122, 21775124, 21705115, 51473136, 21575116), and Natural Science Foundation of Chongqing City (cstc2018jcyjAX0693), China.

References

Bartel, D.P., 2004. Cell 116, 281-297.

Bi, S., Yue, S.Z., Zhang, S.S., 2017. Chem. Soc. Rev. 46, 4281-4298.

Cao, W.D, Ferrance, J.P., Demas, J., Landers, J.P., 2006. J. Am. Chem. Soc. 128, 7572-7578.

Chen, H.M., Lu, Q.Y., Liao, J.Y., Yuan, R., Chen, S.H., 2016. Chem. Commun. 52, 7276-7279.

Chen, H.M., Zhang, H., Yuan, R., Chen, S.H., 2017. Anal. Chem. 89, 2823-2829.

Chen, Y.X., Huang, K.J., Niu, K.X., 2018. Biosens. Bioelectron. 99, 612-624.

Deng, S.Y., Cheng, L.X., Lei, J.P., Cheng, Y., Huang, Y., Ju, H.X., 2013. Nanoscale 5, 5435-5441.

Deng, S. Y., Hou, Z. T., Lei, J. P., Lin, D. J., Hu, Z., Yan, F., Ju, H. X., 2011.

Chem. Commun. 47, 12107-12109.

Ding, H.C., Tang, Z.R., Zhang, L., Dong, Y.P., 2019. The Analyst 144, 1326-1333.

Du, M.X., Du, Y., Feng, Y.B., Li, Z.F., Wang, J.Y., Jiang, N., Liu, Y., 2019. Cellulose. 26, 5543-5557.

Feng, Q.M., Guo, Y.H., Xu, J.J., Chen, H.Y., 2018. Biosens. Bioelectron. 100, 571-576.

Gao, J., Loi, M.A., de Carvalho, E.J.F., Dos Santos, M.C., 2011. ACS Nano 5, 3993-3999.

Gu, Y., Song, J., Li, M.X., Zhang, T.T., Zhao, W., Xu, J.J., Liu, M., Chen, H.Y., 2017. Anal. Chem. 89, 10585-10591.

Huo, X.L., Zhang, N., Yang, H., Xu, J.J., Chen, H.Y., 2018. Anal. Chem. 90, 13723-13728.

Johnson, S.M., Grosshans, H., Shingara, J., Byrom, M., Jarvis, R., Cheng, A., Labourier, E., Reinert, K.L., Brown, D., Slack, F.J., 2005. Cell 120, 635-647.

Kilic, T., Erdem, A., Ozsoz, M., Carrara, S., 2018. Biosens. Bioelectron. 99, 525-546.

Koo, K.M., Carrascosa, L.G., Shiddiky, M.J.A., Trau, M., 2016. Anal. Chem. 88, 2000-2005.

Li, L.L., Chen, Y., Zhu, J.J., 2016. Anal. Chem. 89, 358-371.

Li, Q., Sun, K., Chang, K.W., Yu, J.B., Chiu, D.T., Wu, C.F., Qin, W.P., 2013. Anal. Chem. 85, 9087-9091.

Li, Y.F., Yue, S.Z., Qi, H.J., Ding, C.F., Song, W.L., Bi, S., 2019. Chem. Commun. 55, 4103-4106.

Liang, W.B., Zhuo, Y., Xiong, C.Y., Zheng, Y.N., Chai, Y.Q., Yuan, R., 2017. Biosens. Bioelectron. 94, 568-574.

Liao, H.X., Zhou, Y., Chai, Y.Q., Yuan, R., 2018. Biosens. Bioelectron. 114, 10-14.

Liu, J.L., Tang, Z.L., Zhuo, Y., Chai, Y.Q., Yuan, R., 2017. Anal. Chem. 89, 9108-9115.

Liu, W., Chen, A.Y., Li, S.K., Peng, K.F., Chai, Y.Q., Yuan, R., 2018. Anal. Chem. 91, 1516-1523.

Liu, X.Q., Shi, L.H., Niu, W.X., Li, H.J., Xu, G.B., 2007. Angew. Chem. Int. Ed. 46, 421-424.

Liu, Z.Y., Qi, W.J., Xu, G.B., 2015. Chem. Soc. Rev. 44, 3117-3142.

Lu, H.J., Pan, J.B., Wang, Y.Z., Ji, S.Y., Zhao, W., Luo, X.L., Xu, J.J., Chen, H.Y., 2018. Anal. Chem. 90, 10434-10441.

Lu, J., Wu, L., Hu, Y.F., Wang, S., Guo, Z.Y., 2018. Biosens. Bioelectron. 109, 13-19.

Lu, Q.Y., Zhang, J.J., Wu, Y.Y., Chen, S.H., 2015. RSC Adv. 5, 63650-63654.

Luo, J.H., Li, Q., Chen, S.H., Yuan, R., 2019. ACS Appl. Mater. Interfaces 11, 27363-27370.

Lv, Y.Q., Chen, S.Y., Shen, Y.F., Ji, J.J., Zhou, Q., Liu, S.Q., Zhang, Y.J., 2018. J. Am. Chem. Soc. 140, 2801-2804.

Ma, L., Wu, N., Liu, Y., Ran, X.Q., Xiao, D.B., 2019. Electrochim. Acta 297, 826-832.

Pecher, J., Mecking, S., 2010. Chem. Rev. 110(10), 6260-6279.

Nistri, S., Boccalini, G., Bencini, A., Becatti, M., Valtancoli, B., Conti, L., Lucarini, L., Bani, D., 2015. Free Radical Res. 49, 67-77.

Prieto, I., Teetsov, J., Fox, M.A., Vanden Bout, D.A., Bard, A.J., 2001. J. Phys. Chem. A 105, 520-523.

Qi, H.J., Yue, S.Z., Bi, S., Ding, C.F., Song, W.L., 2018. Chem. Commun. 54, 8498-8501.

Richter, M.M., 2004. Chem. Rev. 104, 3003-3036.

Shan, Y., Xu, J.J., Chen, H.Y., 2009. Chem. Commun. 905-907.

Sun, W., Hayden, S., Jin, Y.H., Rong, Y., Yu, J.B., Ye, F.M., Chan, Y.H., Zeigler, M., Wu, C.F., Chiu, D.T., 2012. Nanoscale 4, 7246.

Tricoli, J.V., Jacobson, J.W., 2007. Cancer Res. 67, 4553-4555.

Wu, C.F., Bull, B., Szymanski, C., Christensen, K., McNeill, J., 2008. ACS Nano 2, 2415-2423.

Yoo, D.Y., Tu, N.D.K., Lee, S.J., Lee, E., Jeon, S., Hwang, S., Lim, H.S., Kim, J.K., Ju, B.K., Kim, H., Lim, J.A., 2014. ACS Nano 8, 4248-4256.

Yu, S., Wang, Y.Y., Jiang, L.P., Bi, S., Zhu, J.J., 2018. Anal. Chem. 90, 4544-4551.

Yue, S.Z., Song, X.Y., Song, W.L., Bi, S., 2019. Chem. Sci. 10, 1651-1658.

Zhang, H., Lu, Q.Y., Zuo, F.M., Yuan, R., Chen, S.H., 2017. Sens. Actuator B: Chem. 241, 887-894.

Zhang, H., Zuo, F.M, Tan, X.R., Xu, S.H., Yuan, R., Chen, S.H., 2018. Biosens. Bioelectron. 104, 65-71.

Zhang, K., Wang, K., Zhu, X., Xu, F., Xie, M.H., 2017. Biosens. Bioelectron. 87,

358-364.

Zhang, P., Jiang, J., Yuan, R., Zhuo, Y., Chai, Y.Q., 2018. J. Am. Chem. Soc. 140, 9361-9364.

Zhang, P., Wu, X., Yuan, R., Chai, Y.Q., 2015. Anal. Chem. 87, 3202-3207.

Zhang, Y., Li, X., Xu, Z.Q., Chai, Y.Q., Wang, H.J., Yuan, R., 2018. Chem. Commun. 54, 10148-10151.

Zhou, H., Zhang, Y.Y., Liu, J., Xu, J.J., Chen, H.Y., 2013. Chem. Commun. (Camb) 49, 2246-2248.

Research Highlights

- A high-intensity OH^--dependent ECL emission of PFO Pdots without any exogenous species or dissolved O_2 as co-reactant was detected.
- The controllability of OH^- concentration in buffer system (PBS) endowed the OH^--dependent ECL emission of PFO Pdots a high stability and repeatability.
- H_2O_2 was found to be highly efficient quencher for the ECL of PFO Pdots.
- The proposed ECL biosensor showed an excellent stability, a satisfactory selectivity and a low detection limit for miRNA-155 detection

Credit Author Statement

Di Liu: Conceptualization; Data curation; Formal analysis; Investigation; Writing - original draft; Writing - review & editing.

Xiaolong Zhang: Data curation; Writing - original draft; Investigation.

Jinwen Zhao: Conceptualization; Supervision.

Shihong Chen: Funding acquisition; Resources; Project administration; Writing - review & editing.

Ruo Yuan: Funding acquisition; Resources; Supervision.

Declaration of interests

☒ The authors declare that they have no known competing financial interests or personal relationships that could have appeared to influence the work reported in this paper.

☐The authors declare the following financial interests/personal relationships which may be considered as potential competing interests: